Ultralight Scalar and Axion Dark Matter Detection with Long-Baseline Atom Interferometers

Wei Zhao(赵伟)[1*], Hui Liu(刘慧)[1], and Xitong Mei(梅希彤)[2,3]

[1]*Shandong University of Aeronautics, Binzhou 256600, China*
[2]*State Key Laboratory of Magnetic Resonance and Atomic and Molecular Physics, Innovation Academy for Precision Measurement Science and Technology, Chinese Academy of Sciences, Wuhan 430071, China*
[3]*University of Chinese Academy of Sciences, Beijing 100049, China*

(Received 1 July 2024; accepted manuscript online 29 October 2024)

Detecting dark matter remains one of the most challenging problems in modern physics. We propose a method to detect the coupling of ultralight scalar dark matter to quarks and gluons, as well as the coupling of ultralight axion dark matter to gluons, using long-baseline atom interferometers. Interactions between ultralight scalar and axion dark matter with quarks and gluons can induce oscillations in nuclear charge radii, consequently causing oscillations in atomic transition frequencies. We calculate the differential phase shift produced by these dark matter interactions in long-baseline atom interferometers, presenting constraints on the scalar dark matter coupling parameters d_g and $d_{\hat{m}}$, as well as on the axion dark matter coupling parameter $1/f_a$. Our results are anticipated to improve existing bounds and complement bounds from other experiments.

DOI: 10.1088/0256-307X/41/12/129501

1. Introduction. There is substantial evidence supporting the existence of dark matter (DM),[1–3] however, no direct DM signal has yet been detected,[4,5] making DM detection a significant challenge in modern physics. Ultralight DM represents an important class of DM candidates, including scalar DM, axion DM, and dark photon DM, with masses ranging from 10^{-22} eV to 1 eV.[6–9] An increasing number of experiments and proposals are being developed to search for these DM candidates, utilizing techniques such as accelerometers,[10] atomic clocks,[11,12] and laser interferometers.[13–15]

Atom interferometers (AIs) operate by manipulating atomic matter waves[16] and are widely applied across various fields,[17] such as fine structure constant measurement,[18] weak equivalence principle test,[19,20] and gravitational wave detection.[21] Recently, several long-baseline AI schemes have been proposed,[22] such as AION,[23] MAGIS-100,[24] MIGA,[25] ELGAR,[26] ZAIGA,[27] and AEDGE,[28] which presents new opportunities to detect ultralight DM with AIs. Various proposals have been introduced to leverage AIs for DM detection in previous works,[22,29–39] exploring signals from changes in the fine structure constant, electron mass, and acceleration due to DM.

In the ultralight scalar DM model, scalar DM can interact with the electromagnetic field, gluons, electrons, and quarks, with corresponding interaction strengths represented by five coupling parameters: d_e, d_g, d_{m_e}, $d_{\hat{m}}$ and $d_{\delta m}$. In the ultralight axion DM model, axion DM interacts specifically with gluons, with the interaction strength characterized by the parameter $1/f_a$. In this Letter, we consider the oscillation of atomic energy levels induced by oscillations in nuclear charge radii,[40–43] which manifests as a differential phase shift in long-baseline AIs. We calculate the differential phase shifts caused by scalar and axion DM interaction separately. Since these nuclear charge radius oscillations are related to the scalar DM coupling parameters d_g and $d_{\hat{m}}$ as well as the axion DM coupling parameter $1/f_a$, we can constrain these coupling parameters by using long-baseline AIs. Our results provide complementary insights to existing experimental schemes.[10–12,14,15,30,41,44–47]

This study is organized as follows. In Section 2, we introduce the ultralight scalar DM and axion DM models. Section 3 discusses the signals produced by scalar and axion DM in long-baseline AIs. In Section 4, we present constraints on the coupling parameters between DM and standard model particles. Section 5 provides the conclusion.

2. The Dark Matter Model.

2.1. The Scalar Dark Matter Model. In the scalar DM model, we consider the following interaction Lagrangian density between scalar DM and standard model particles[48,49]

$$\mathcal{L}_{\rm int} = \varphi\Big[\frac{d_e}{4e^2}F_{\mu\nu}F^{\mu\nu} - \frac{d_g\beta_3}{2g_3}F^A_{\mu\nu}F^{A\mu\nu} - \sum_{i=e,u,d}(d_{m_i}+\gamma_{m_i}d_g)m_i\bar{\psi}_i\psi_i\Big], \quad (1)$$

where d_e, d_g, d_{m_e}, d_{m_u}, and d_{m_d} are the coupling parameters by which scalar DM interacts with the electromagnetic field, gluon field, electrons, up quarks, and down quarks. Here, β_3 is the β-function for g_3, m_i denotes the masses of electrons and quarks, γ_{m_i} represents the anomalous dimension due to the renormalization-group running of quark masses, and ψ_i are the fermion fields. The scalar

*Corresponding author. Email: zhaowei164@mails.ucas.ac.cn
© 2024 Chinese Physical Society and IOP Publishing Ltd

DM field φ is treated as a classical field

$$\varphi = \varphi_0 \cos(\omega_\varphi t + \delta), \tag{2}$$

where $\varphi_0 = \frac{\sqrt{2\rho_{\rm DM}}}{m_\varphi E_{\rm P}} \simeq 7 \times 10^{-31}\,{\rm eV/m_\varphi}$ represents the scalar DM amplitude, $\rho_{\rm DM} = 0.4\,{\rm GeV/cm^3}$ is the local DM energy density, $E_{\rm P}$ is the reduced Planck energy, $\omega_\varphi \simeq m_\varphi c^2/\hbar$ denotes the scalar DM frequency, m_φ is the scalar DM mass, and δ is the initial phase. In some literatures, a dimensional scalar field ϕ is used, with the relationship $\phi = \varphi E_{\rm P}$. The corresponding coupling parameters are defined as $\Lambda_\gamma = E_{\rm P}/d_e$, $\Lambda_g = E_{\rm P}/d_g$, and $\Lambda_i = E_{\rm P}/d_{m_i}$.[49]

Following a detailed analysis,[48] the Lagrangian in Eq. (1) can induce oscillations in five key physical quantities, governed by φ, as follows:

$$\begin{aligned} &\alpha(\varphi) = (1 + d_e\varphi)\alpha, \quad \Lambda_{\rm QCD}(\varphi) = (1 + d_g\varphi)\Lambda_{\rm QCD}, \\ &m_i(\varphi) = (1 + d_{m_i}\varphi)m_i, \quad i = e, u, d, \end{aligned} \tag{3}$$

where α denotes the electromagnetic fine structure constant and $\Lambda_{\rm QCD}$ is the QCD energy scale. The implications of variations in fine structure constant and electron mass in AI experiments have already been examined in previous works.[22,30] In this study, we focus on additional effects not previously discussed. To simplify analysis, the quark masses could be expressed as symmetric and antisymmetric combinations

$$\hat{m} = \frac{m_u + m_d}{2}, \quad \delta m = m_d - m_u. \tag{4}$$

The corresponding dependence on scalar DM is

$$\hat{m}(\varphi) = (1 + d_{\hat{m}}\varphi)\hat{m}, \quad \delta m(\varphi) = (1 + d_{\delta m}\varphi)\delta m, \tag{5}$$

where

$$d_{\hat{m}} = \frac{m_u d_{m_u} + m_d d_{m_d}}{m_u + m_d}, \quad d_{\delta m} = \frac{m_d d_{m_d} - m_u d_{m_u}}{m_d - m_u}. \tag{6}$$

It is known that the pion mass is related to the quark mass and the QCD energy scale, following the relationship $m_\pi^2 \propto \Lambda_{\rm QCD}\,\hat{m}$.[50] Consequently, the oscillation of the quark mass and the QCD energy scale induces a corresponding variation in the pion mass as[44]

$$\frac{\Delta m_\pi^2}{m_\pi^2} = (d_g + d_{\hat{m}})\varphi. \tag{7}$$

2.2. The Axion Dark Matter Model. In this section, we examine the interaction between axion DM and gluons, represented by the interaction Lagrangian:

$$\mathcal{L}_{\rm int} = \frac{g_s^2}{32\pi^2}\frac{a}{f_a}F^A_{\mu\nu}\tilde{F}^{A\mu\nu}, \tag{8}$$

where g_s denotes the strong coupling constant, f_a represents the axion decay constant, and $\tilde{F}^{A\mu\nu}$ is the dual gluon field strength. The axion DM field, denoted by a, is further characterized by

$$a = a_0 \cos(\omega_a t + \delta), \tag{9}$$

where $a_0 = \sqrt{2\rho_{\rm DM}}/m_a \simeq 0.0024\,({\rm eV})^2/m_a$ represents the axion DM amplitude, with $\omega_a \simeq m_a c^2/\hbar$ as the axion DM frequency, m_a as the axion DM mass, and δ as the initial phase. The interaction of axion DM with hadrons can also induce oscillations in the pion mass, as discussed in Ref. [44]

$$\frac{\Delta m_\pi^2}{m_\pi^2} \simeq -\frac{m_u m_d}{2(m_u + m_d)^2}\,\theta_{\rm eff}^2(t) = -\frac{m_u m_d}{2(m_u + m_d)^2}\frac{1}{f_a^2}a^2, \tag{10}$$

where $m_u = 2.16\,{\rm MeV}$ and $m_d = 4.67\,{\rm MeV}$ represents the masses of up and down quarks, respectively.[51]

3. The Dark Matter Signal in Atom Interferometers. Here, we briefly outline the principle of a typical $\pi/2 - \pi - \pi/2$ light pulse AI.[52,53] More detailed descriptions are available in several studies, such as Refs. [16,17]. Initially, at $t = 0$, a $\pi/2$-pulse is applied to split the atomic wave packet in the ground state into a superposition of ground and excited states. At time $t = T$, a π-pulse redirects the atomic packets in these states. Finally, at $t = 2T$, a $\pi/2$-pulse recombines the two atomic beams, enabling phase shift measurement through the detection of atom populations in the ground or excited state. In this study, we focus on long-baseline AIs controlled by a common laser, with an arm length $L \simeq x_2 - x_1$, as depicted in Fig. 1. The common laser configuration effectively cancels out laser phase noise, and the DM signal is detected by measuring the differential phase shift between the two AIs.

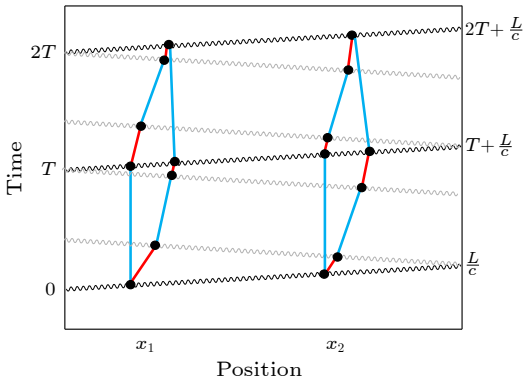

Fig. 1. Schematic diagram for long-baseline AIs. Two AIs are positioned at x_1 and x_2. Blue and red lines represent atomic paths, while wavy lines indicate laser pulses. This example illustrates a setup with a large momentum transfers $n = 2$.

The shift in atomic energy levels due to the mass shift and the field shift-related to the finite nucleus mass and nuclear charge radius-can be expressed as[54]

$$E_{\rm total} = E_{\rm MS} + E_{\rm FS} = K\frac{1}{m_N} + F\langle r_N^2\rangle, \tag{11}$$

where K is the mass shift factor, F is the field shift factor, m_N denotes the nucleon mass, and $\langle r_N^2\rangle$ represents the mean squared nuclear charge radius.

The change in the atomic energy level shift is given by

$$\begin{aligned} \Delta E_{\rm total} &= \Delta E_{\rm MS} + \Delta E_{\rm FS} \\ &= K\frac{1}{m_N}\frac{\Delta m_N}{m_N} + F\langle r_N^2\rangle\frac{\Delta\langle r_N^2\rangle}{\langle r_N^2\rangle} \\ &\simeq F\langle r_N^2\rangle\frac{\Delta\langle r_N^2\rangle}{\langle r_N^2\rangle}. \end{aligned} \tag{12}$$

For heavy nuclei, such as those in Yb atoms, the field shift predominates.[44] Thus, we derive the corresponding change in the transition frequency as follows:

$$\Delta\omega_A = \tilde{F}\langle r_N^2\rangle \frac{\Delta\langle r_N^2\rangle}{\langle r_N^2\rangle}, \tag{13}$$

where $\tilde{F}$ represents the differential field shift factor between the excited state and the ground state. In this study, we focus on the $^1S_0 - ^3P_0$ clock transition of the Yb atom, with $\tilde{F} = 2\pi \times 10.852\,\mathrm{GHz/fm^2}$ [55] and a nuclear radius $r_N = 5.3\,\mathrm{fm}$.[56] The Yb atom provides enhanced sensitivity due to its larger field shift factor compared to lighter atoms, which generally exhibit smaller values.[57,58] The variation in the nuclear charge radius is related to the pion decay constant f_π, the pion mass m_π, and nucleon interactions. Detailed relationships between $\langle r_N^2\rangle$ and both f_π and m_π are available in Ref. [44] as

$$\begin{aligned}\frac{\Delta\langle r_N^2\rangle}{\langle r_N^2\rangle} &\simeq \alpha\frac{\Delta f_\pi}{f_\pi} + \beta\frac{\Delta m_\pi^2}{m_\pi^2} \\ &\simeq \alpha\frac{\Delta\Lambda_{\mathrm{QCD}}}{\Lambda_{\mathrm{QCD}}} + \beta\frac{\Delta m_\pi^2}{m_\pi^2},\end{aligned} \tag{14}$$

where $\alpha = -2$, $\beta = -0.2$.

3.1. The Scalar Dark Matter Signal in Atom Interferometers. Scalar dark matter interacts with quarks and gluons, inducing oscillations in the QCD energy scale and pion mass. By substituting Eq. (3) and Eq. (7) into Eq. (14), we obtain the effect of scalar DM on the nuclear charge radius as follows:

$$\frac{\Delta\langle r_N^2\rangle}{\langle r_N^2\rangle} \simeq (\alpha+\beta)d_g\varphi + \beta d_{\hat{m}}\varphi. \tag{15}$$

The oscillation in the nuclear charge radius induces a corresponding oscillation in the atomic transition frequency, expressed as:

$$\Delta\omega_A(t) = \tilde{F}\langle r_N^2\rangle[(\alpha+\beta)d_g + \beta d_{\hat{m}}]\varphi_0\cos(\omega_\varphi t + \delta). \tag{16}$$

This oscillation in atomic transition frequency, driven by DM, causes a phase shift accumulation in the excited state atoms relative to the ground state atoms. Here, we neglect the atomic size and the spatial variation of the DM field, as these are minor compared to the size of AIs and the temporal DM signals, respectively. This influence of DM on photon propagation is also disregarded, as it does not affect the speed or frequency of laser light.[30] By measuring the differential phase shift between two AIs, the signal of scalar DM could be extracted as follows:[22,30]

$$\begin{aligned}\Phi_{\mathrm{eng}} = &\int_{T-(n-1)\frac{L}{c}}^{T+\frac{L}{c}} \Delta\omega_A(t)dt - \int_0^{\frac{nL}{c}} \Delta\omega_A(t)dt \\ &- \int_{2T-(n-1)\frac{L}{c}}^{2T+\frac{L}{c}} \Delta\omega_A(t)dt + \int_T^{T+\frac{nL}{c}} \Delta\omega_A(t)dt.\end{aligned} \tag{17}$$

Following a detailed calculation, the differential phase shift induced by the scalar DM is obtained as

$$\begin{aligned}\Phi^s_{\mathrm{eng}} = &\frac{\tilde{F}\langle r_N^2\rangle[(\alpha+\beta)d_g + \beta d_{\hat{m}}]\varphi_0}{\omega_\varphi} \\ &\times\Big[\sin\Big[\omega_\varphi\Big(T+\frac{L}{c}\Big)+\delta\Big] - \sin\Big[\omega_\varphi\Big(T-(n-1)\frac{L}{c}\Big)+\delta\Big] \\ &- \sin\Big[\frac{\omega_\varphi nL}{c}+\delta\Big] + \sin[\delta] - \sin\Big[\omega_\varphi\Big(2T+\frac{L}{c}\Big)+\delta\Big] \\ &+ \sin\Big[\omega_\varphi\Big(2T-(n-1)\frac{L}{c}\Big)+\delta\Big] + \sin\Big[\omega_\varphi\Big(T+\frac{nL}{c}\Big)+\delta\Big] \\ &- \sin[\omega_\varphi T+\delta]\Big].\end{aligned} \tag{18}$$

From Eq. (18), it is evident that the strength of the DM signal is linearly proportional to the coupling parameters d_g and $d_{\hat{m}}$. This implies that long-baseline AIs can be employed to detect the coupling of scalar DM to gluons and quarks. The signal's magnitude also depends on the specific atomic species used, as variations in field shift and nuclear charge radius impact the outcome.

3.2. The Axion Dark Matter Signal in Atom Interferometers. Axion DM interacts with gluons, resulting in oscillations in the pion mass and consequently altering the nuclear charge radius. By substituting Eq. (10) into Eq. (14), we obtain the change in nuclear charge radius:

$$\frac{\Delta\langle r_N^2\rangle}{\langle r_N^2\rangle} \simeq -\frac{\beta m_u m_d}{2(m_u+m_d)^2}\frac{1}{f_a^2}a^2, \tag{19}$$

and the corresponding oscillation in the atomic transition frequency is defined as follows:

$$\Delta\omega_A = -\tilde{F}\langle r_N^2\rangle\frac{\beta m_u m_d}{2(m_u+m_d)^2}\frac{1}{f_a^2}a_0^2\cos^2(\omega_a t+\delta). \tag{20}$$

Similar to the scalar DM, by substituting Eq. (20) into Eq. (17), we derive the differential phase shift induced by the axion DM as follows:

$$\begin{aligned}\Phi^a_{\mathrm{eng}} = &-\tilde{F}\langle r_N^2\rangle\frac{\beta m_u m_d}{2(m_u+m_d)^2}\frac{a_0^2}{f_a^2}\frac{1}{4\omega_a} \\ &\times\Big[\sin\Big[2\omega_a\Big(T+\frac{L}{c}\Big)+2\delta\Big] \\ &- \sin\Big[2\omega_a\Big(T-(n-1)\frac{L}{c}\Big)+2\delta\Big] \\ &- \sin\Big[\frac{2\omega_a nL}{c}+2\delta\Big] + \sin[2\delta] \\ &- \sin\Big[2\omega_a\Big(2T+\frac{L}{c}\Big)+2\delta\Big] \\ &+ \sin\Big[2\omega_a\Big(2T-(n-1)\frac{L}{c}\Big)+2\delta\Big] \\ &+ \sin\Big[2\omega_a\Big(T+\frac{nL}{c}\Big)+2\delta\Big] \\ &- \sin\Big[2\omega_a T+2\delta\Big]\Big].\end{aligned} \tag{21}$$

From Eq. (21), we observe that the axion DM signal depends quadratically on the coupling parameter $1/f_a$. This quadratic dependence enables the detection of axion DM coupling to gluons using long-baseline AIs.

4. Constraints on The Coupling Parameters. The facility's sensitivity depends on several technical parameters of the AIs, including arm length L, free evolution time T, and the number of large momentum transfers n. For underground long-baseline AIs, we assume

$L = 3 \times 10^3$ m, $T = 1.4$ s, and $n = 4 \times 10^4$. With advancements in technology, we anticipate further enhancement in phase sensitivity through increased atomic flux density and the application of squeezed atomic states.[59,60] This could potentially bring phase sensitivity to the level of $10^{-6}/\text{Hz}^{1/2}$.[22,23,27] Additionally, greater arm lengths L and extended free evolution time T, achievable in space-based experiments, could yield even better sensitivity. For space-based long-baseline AIs, the arm length is expected to be approximately $L \simeq 10^7$ m, with a free evolution time potentially reaching $T \simeq 10^2$ s. Phase sensitivity could be as high as $10^{-5}/\text{Hz}^{1/2}$. Large momentum transfer numbers on the order of $n \simeq 10^3$ have already been demonstrated experimentally.[61,62] In terms of noise, shot noise is intrinsic and typically dominates at the frequencies above 10^{-1} Hz for underground long-baseline AIs and above 10^{-4} Hz for space-based long-baseline AIs.[30] For this study, we consider only shot noise, assuming an ideal signal-to-noise ratio (SNR = 1) after an integration time of $t_{\text{int}} \simeq 10^8$ s.[22,30] Our proposed search method operates in a broadband mode using single photon transitions, aiming to cover a wider frequency range of DM.[22,63]

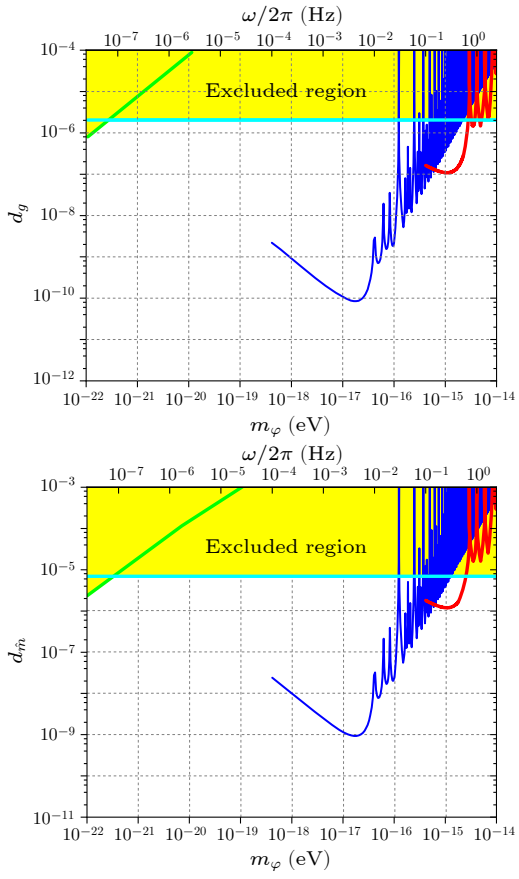

Fig. 2. Constraints on the scalar DM coupling parameters d_g and $d_{\hat{m}}$. The red and blue lines indicate the constraints on d_g and $d_{\hat{m}}$ derived from underground and space-based AIs, respectively. The yellow regions denote exclusions from MICROSCOPE experiments, highlighted by cyan lines[47,64,65], and atomic spectroscopy experiments, marked by green lines.[44,66,67] The sensitivity cutoffs on the red and blue lines at lower masses are due to the increasing dominance of gravitational gradient noise.

4.1. Constraints on the Scalar Dark Matter. Using these technological parameters, we constrain one coupling parameter at a time, setting the others to zero. Given the oscillatory nature of the initial phase δ, we use the signal amplitude $\bar{\Phi}^s_{\text{eng}} = [2\int_0^{2\pi}(\Phi^s_{\text{eng}})^2/2\pi d\delta]^{1/2}$ to establish constraints on the coupling parameters. Figure 2 shows the proposed constraints on the scalar DM coupling parameters d_g and $d_{\hat{m}}$, represented by red lines for underground AIs and blue lines for space-based AIs. The yellow regions indicate exclusions by MICROSCOPE and atomic spectroscopy experiments. These constraints surpass MICROSCOPE results by several orders of magnitude, particularly at $m_\varphi = 10^{-15}$ eV and $m_\varphi = 10^{-17}$ eV, where sensitivity is optimal for underground and space-based AIs, respectively. This peak sensitivity is influenced by the trigonometric functions in the phase shift, which depend on T, n, L, determining the resonant frequency.

Our results complement those of atomic spectroscopy experiments,[12,44,66,67] which primarily constrain coupling parameters at lower frequencies. Our approach also diverges from previous AI experiments aimed at detecting scalar DM. In Ref. [29], the DM signal is observed through variations in Earth's gravitational field, yielding sensitivity at lower frequencies. Ref. [30] provides constraints on scalar DM coupling parameters d_e and d_{m_e} by examining oscillations in atomic transition frequencies, while Ref. [39] constrains scalar DM coupling parameters by comparing accelerations of different atomic species. In contrast, our proposal focuses on constraining scalar DM parameters d_g and $d_{\hat{m}}$ by leveraging oscillations in transition frequencies induced by scalar DM interactions with quarks and gluons, using a single atomic species.

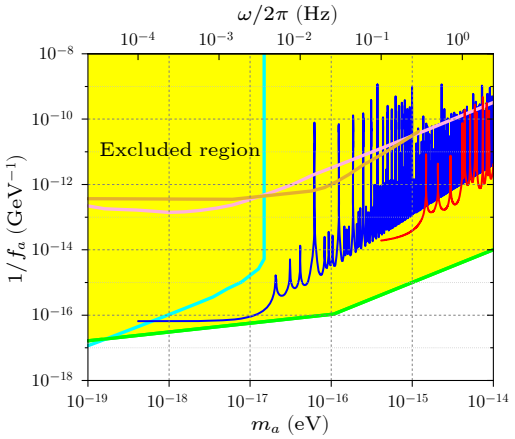

Fig. 3. Constraints on the axion DM coupling parameter $1/f_a$. The red and blue lines represent constraints on $1/f_a$ from underground and space-based AIs, respectively. The yellow regions indicate exclusions from various experiments: the oscillating neutron electric dipole moment experiment (cyan line),[45] the Beam EDM experiment (pink line),[46] the MICROSCOPE experiment (orange line),[47] and the BBN (green line).[68] The sensitivity cutoffs on the red and blue lines at lower masses result from the increased influence of gravitational gradient noise.

4.2. Constraints on the Axion Dark Matter. Similar to the scalar DM, we can constrain the axion DM coupling

parameter $1/f_a$ using $\bar{\Phi}^a_{\rm eng} = \left[2\int_0^{2\pi}\left(\Phi^a_{\rm eng}\right)^2/2\pi d\delta\right]^{1/2}$. In Fig. 3, the red and blue lines represent our proposed constraints on $1/f_a$ from underground and space-based AIs, respectively, while the yellow region shows exclusions from other experiments.[45–47,68] Our approach differs from previous AI experiments targeting axion DM. For example, Refs. [37,38] provide constraints by examining quadratic interactions between the axion and the electromagnetic field or electrons, while Ref. [39] constrains the axion coupling parameter by comparing accelerations of different atomic species. In contrast, our constraints are based on the interaction between the axion and gluons, utilizing a single atomic species.

5. Conclusion. In this study, we propose a method for detecting ultralight scalar and axion DM using long-baseline AIs, focusing on the coupling interactions between DM and quarks and gluons. We calculate the differential phase shifts induced by ultralight scalar and axion DM in long-baseline AIs. We further present proposed constraints on the scalar DM coupling parameters d_g and $d_{\hat{m}}$ as well as the axion DM coupling parameter $1/f_a$. Our findings are anticipated to enhance current bounds and provide complementary constraints alongside other experimental results. With advancing detection sensitivity, these methods are expected to reveal further insights into the properties of DM.

Acknowledgements. This work was supported by the Shandong Provincial Natural Science Foundation (Grant No. ZR2023QA143) and the Startup Foundation for Doctors of Shandong University of Aeronautics (Grant No. 2022Y18).

References

[1] Rubin V C, Ford W K Jr, and Thonnard N 1978 *Astrophys. J.* **225** L107
[2] Allen S W, Schmidt R W, Fabian A C, and Ebeling H 2003 *Mon. Not. R. Astron. Soc.* **342** 287
[3] Clowe D, Bradač M, Gonzalez A H, Markevitch M, Randall S W, Jones C *et al.* 2006 *Astrophys. J.* **648** L109
[4] Meng Y, Wang Z, Tao Y *et al.* (PandaX-4T Collaboration) 2021 *Phys. Rev. Lett.* **127** 261802
[5] Aalbers J, Akerib D S, Akerlof C W *et al.* (LUX-ZEPLIN Collaboration) 2023 *Phys. Rev. Lett.* **131** 041002
[6] Battaglieri M, Belloni A, Chou A *et al.* 2017 arXiv:1707.04591
[7] Safronova M S, Budker D, DeMille D, Jackson Kimball D F, Derevianko A, and Clark C W 2018 *Rev. Mod. Phys.* **90** 025008
[8] Antypas D, Banerjee A, Bartram C *et al.* 2022 arXiv:2203.14915
[9] Adams C B, Aggarwal N, Agrawal A *et al.* 2022 arXiv:2203.14923
[10] Graham P W, Kaplan D E, Mardon J, Rajendran S, and Terrano W A 2016 *Phys. Rev. D* **93** 075029
[11] Arvanitaki A, Huang J, and Van Tilburg K 2015 *Phys. Rev. D* **91** 015015
[12] Beloy K *et al.* (BACON Collaboration) 2021 *Nature* **591** 564
[13] Stadnik Y V and Flambaum V V 2015 *Phys. Rev. Lett.* **114** 161301
[14] Grote H and Stadnik Y V 2019 *Phys. Rev. Research* **1** 033187
[15] Vermeulen S M, Relton P, Grote H *et al.* 2021 *Nature* **600** 424
[16] Cronin A D, Schmiedmayer J, and Pritchard D E 2009 *Rev. Mod. Phys.* **81** 1051
[17] Tino G M 2021 *Quantum Sci. Technol.* **6** 024014
[18] Morel L, Yao Z B, Cladé P, and Guellati-Khélifa S 2020 *Nature* **588** 61
[19] Asenbaum P, Overstreet C, Kim M, Curti J, and Kasevich M A 2020 *Phys. Rev. Lett.* **125** 191101
[20] Elliott E R, Aveline D C, Bigelow N P *et al.* 2023 *Nature* **623** 502
[21] Dimopoulos S, Graham P W, Hogan J M, Kasevich M A, and Rajendran S 2008 *Phys. Rev. D* **78** 122002
[22] Abend S, Allard B, Alonso I, Antoniadis J, Araújo H, Arduini G *et al.* 2024 *AVS Quantum Science* **6** 024701
[23] Badurina L, Bentine E, Blas D, Bongs K, Bortoletto D, Bowcock T *et al.* 2020 *J. Cosmol. Astropart. Phys.* **2020** 011
[24] Abe M, Adamson P, Borcean M *et al.* 2021 *Quantum Sci. Technol.* **6** 044003
[25] Canuel B, Bertoldi A, Amand L *et al.* 2018 *Sci. Rep.* **8** 14064
[26] Canuel B, Abend S, Amaro-Seoane P *et al.* 2020 *Class. Quantum Grav.* **37** 225017
[27] Zhan M S, Wang J, Ni W T *et al.* 2020 *Int. J. Mod. Phys. D* **29** 1940005
[28] El-Neaj Y A, Alpigiani C, Amairi-Pyka S *et al.* 2020 *EPJ Quantum Technol.* **7** 6
[29] Geraci A A and Derevianko A 2016 *Phys. Rev. Lett.* **117** 261301
[30] Arvanitaki A, Graham P W, Hogan J M, Rajendran S, and Van Tilburg K 2018 *Phys. Rev. D* **97** 075020
[31] Badurina L, Blas D, and McCabe C 2022 *Phys. Rev. D* **105** 023006
[32] Di Pumpo F, Friedrich A, Geyer A, Ufrecht C, and Giese E 2022 *Phys. Rev. D* **105** 084065
[33] Du Y, Murgui C, Pardo K, Wang Y, and Zurek K M 2022 *Phys. Rev. D* **106** 095041
[34] Zhao W, Mei X, Gao D, Wang J, and Zhan M 2022 *Int. J. Mod. Phys. D* **31** 2250037
[35] Zhao W, Gao D, Wang J, and Zhan M 2022 *Gen. Relativ. Gravit.* **54** 41
[36] Di Pumpo F, Friedrich A, and Giese E 2024 *AVS Quantum Sci.* **6** 014404
[37] Beadle C, Ellis S A R, Quevillon J, and Vuong P N H 2023 arXiv:2307.10362
[38] Kim H, Lenoci A, Perez G, and Ratzinger W 2024 *Phys. Rev. D* **109** 015030
[39] Gué J, Hees A, and Wolf P 2024 *Phys. Rev. D* **110** 035005
[40] Flambaum V V and Mansour A J 2023 *Phys. Rev. Lett.* **131** 113004
[41] Flambaum V V and Samsonov I B 2023 *Phys. Rev. D* **108** 075022
[42] Dzuba V A and Flambaum V V 2023 *Phys. Rev. Lett.* **131** 263002
[43] Kim H and Perez G 2024 *Phys. Rev. D* **109** 015005
[44] Banerjee A, Budker D, Filzinger M *et al.* 2023 arXiv:2301.10784
[45] Abel C, Ayres N J, Ban G *et al.* 2017 *Phys. Rev. X* **7** 041034
[46] Schulthess I, Chanel E, Fratangelo A *et al.* 2022 *Phys. Rev. Lett.* **129** 191801
[47] Touboul P, Métris G, Rodrigues M *et al.* (MICROSCOPE Collaboration) 2022 *Phys. Rev. Lett.* **129** 121102
[48] Damour T and Donoghue J F 2010 *Phys. Rev. D* **82** 084033
[49] Hees A, Minazzoli O, Savalle E, Stadnik Y V, and Wolf P 2018 *Phys. Rev. D* **98** 064051
[50] Ubaldi L 2010 *Phys. Rev. D* **81** 025011
[51] Workman R L, Burkert V D, Crede V *et al.* (Particle Data Group) 2022 *Prog. Theor. Exp. Phys.* **2022** 083C01
[52] Kasevich M and Chu S 1991 *Phys. Rev. Lett.* **67** 181
[53] Kasevich M and Chu S 1992 *Appl. Phys. B* **54** 321
[54] Krane K 1991 *Introductory Nuclear Physics* (Wiley)
[55] Schelfhout J S and McFerran J J 2021 *Phys. Rev. A* **104** 022806
[56] Angeli I and Marinova K P 2013 *At. Data Nucl. Data Tables* **99** 69

[57] Dzuba V A, Johnson W R, and Safronova M S 2005 *Phys. Rev. A* **72** 022503
[58] Miyake H, Pisenti N C, Elgee P K, Sitaram A, and Campbell G K 2019 *Phys. Rev. Res.* **1** 033113
[59] Hosten O, Engelsen N J, Krishnakumar R, and Kasevich M A 2016 *Nature* **529** 505
[60] Cox K C, Greve G P, Weiner J M, and Thompson J K 2016 *Phys. Rev. Lett.* **116** 093602
[61] Chiow S W, Kovachy T, Chien H C, and Kasevich M A 2011 *Phys. Rev. Lett.* **107** 130403
[62] Rudolph J, Wilkason T, Nantel M *et al.* 2020 *Phys. Rev. Lett.* **124** 083604
[63] Badurina L, Beniwal A, and McCabe C 2023 *Phys. Rev. D* **108** 083016
[64] Touboul P, Métris G, Rodrigues M *et al.* (MICROSCOPE Collaboration) 2017 *Phys. Rev. Lett.* **119** 231101
[65] Bergé J, Brax P, Métris G, Pernot-Borràs M, Touboul P, and Uzan J P 2018 *Phys. Rev. Lett.* **120** 141101
[66] Hees A, Guéna J, Abgrall M, Bize S, and Wolf P 2016 *Phys. Rev. Lett.* **117** 061301
[67] Kobayashi T, Takamizawa A, Akamatsu D *et al.* 2022 *Phys. Rev. Lett.* **129** 241301
[68] Blum K, D'Agnolo R T, Lisanti M, and Safdi B R 2014 *Phys. Lett. B* **737** 30